Non-Linear Output-Conductance Function for Robust Analysis of Two-Dimensional Transistors

Guoli Li, Zizheng Fan, Nicolas André, *Member, IEEE*, Yongye Xu, Ying Xia, Benjamín Iñíguez, *Fellow, IEEE*, Lei Liao, *Senior Member, IEEE*, and Denis Flandre, *Senior Member, IEEE*

***Abstract*— In this work, we explore the output-conductance function (G-function) to interpret the device characteristics of two-dimensional (2D) semiconductor transistors. Based on analysis of the device output conductance, the carrier mobility, and the channel as well as contact resistance are extracted. Thereafter the current-voltage (IV) characteristics of black phosphorous (BP) and MoS_2 transistors from room to low temperature are modeled and compared to experiments. The G-function model proves its reliability and accuracy in parameter extraction and IV modeling of 2D transistors, regardless of the n- or p- type, the short- or long-channel and the Schottky or Ohmic contact. Moreover, this works shows its high potential in the device modeling and further circuit design of the 2D transistors, requiring only few parameters and simulating precise IV characteristics.**

***Index Terms*— Two-dimensional (2D) transistor, output conductance, low temperature, contact resistance, carrier mobility, Schottky contact.**

I. Introduction

TWO-DIMENSIONAL (2D) semiconductor field-effect transistors (FETs) have attracted large interest, owing to the reasonable high carrier mobility, the dangling bond-free surface *etc.* of 2D materials like graphene, black phosphorous (BP) and MoS_2 [1]–[5]. However, the difficulty to dope the 2D semiconductors and the existence of intrinsic defects could lead to high contact resistance as well as contact barrier, which are crucial for precisely interpreting the device characteristics and extracting the corresponding parameters, *e.g.* carrier mobility, threshold voltage [6]–[8]. Arguments have often arisen while using transfer-line method (TLM), transconductance Y function or output-conductance G function [9]–[11]. Several (at least two) different lengths need to be constructed to extract contact resistance in TLM, while keeping all other details the same; on the other hand, in Y-function model, the contact resistance can not be exactly excluded while extracting the carrier mobility. Thereafter, the mobility can be overestimated or underestimated owing to effect of the contact barrier and resistance effect, so that excessive parameters dispersions and deviations were reported [12], [13].

In this letter, for the accurate parameter extraction and device modeling, a universal non-linear G-function method has been explored in the 2D transistors. And, the contact (R_c) and channel resistances (R_{ch}), the mobility (μ) and the threshold voltage (V_{th}) are extracted by simply measuring a output curve in the linear region [11] (Section II). Both simulations and experiments are compared in order to demonstrate that this approach provides physical insight as well as reliable parameter extraction (Section III), for robust analysis of the Ohmic and Schottky contact, the short- and long-channel, and the n- and p-type 2D transistors in a wide range of temperatures and materials.

II. Physical Fundamental and Methodology

A. Output Characteristics in 2D Transistors

Bottom-gated 2D transistors have been fabricated and measured in [12], [14]–[16], where the source electrode is grounded ($V_s = 0$ V). Fig. 1 depicts the output curves (I_d-V_d) and the corresponding output conductance($G = I_d/V_d$) of a BP transistor with channel length of 3.0 μm, operating at room temperature (RT) of 298 K and low temperature (LT) of 11 K. The BP flake was mechanically exfoliated from the bulk BP crystal, and transferred onto a heavily p-doped Si substrate with a 30 nm-thick HfO_2 dielectric [12]. The non-ohmic injection (*e.g.* Schottky barrier contact) is formed in the BP transistor, leading to the bell-shaped G curves at LT are observed in Fig. 1d. Similar Schottky barrier diode (SBD) effect was also observed in MoS_2 transistors [8], [14]. In such cases, how to extend the general approach of G-function model to precisely interpret the device performances, regardless of the contact barrier or resistance? That remains unknown to our best knowledge, and

Manuscript received October 29, 2020; revised November 17, 2020 and November 25, 2020; accepted November 26, 2020. Date of publication December 3, 2020; date of current version December 24, 2020. This work was supported in part by the National Key Research and Development Program of China under Grant 2018YFA0703700; in part by the National Natural Science Foundation of China under Grant 61925403, Grant 61851403, and Grant 62004065; in part by the Hunan Natural Science Foundation under Grant 2020JJ5087; and in part by the Technology Program (Major Project) of Changsha under Grant kq1902042. The review of this letter was arranged by Editor G. Han. *(Corresponding author: Guoli Li.)*

Guoli Li, Zizheng Fan, Yongye Xu, Ying Xia, and Lei Liao are with the Key Laboratory for Micro/Nano-Optoelectronic Devices, Ministry of Education, School of Physics and Electronics, Hunan University, Changsha 410082, China (e-mail: liguoli_lily@hnu.edu.cn).

Nicolas André and Denis Flandre are with the Institute of Information and Communication Technologies, Electronics and Applied Mathematics, Université catholique de Louvain, B-1348 Louvain-la-Neuve, Belgium.

Benjamín Iñíguez is with the Departament d'Enginyeria Electrònica, Elèctrica i Automàtica, Universitat Rovira i Virgili, 43007 Tarragona, Spain.

Color versions of one or more figures in this letter are available at https://doi.org/10.1109/LED.2020.3042212.

Digital Object Identifier 10.1109/LED.2020.3042212

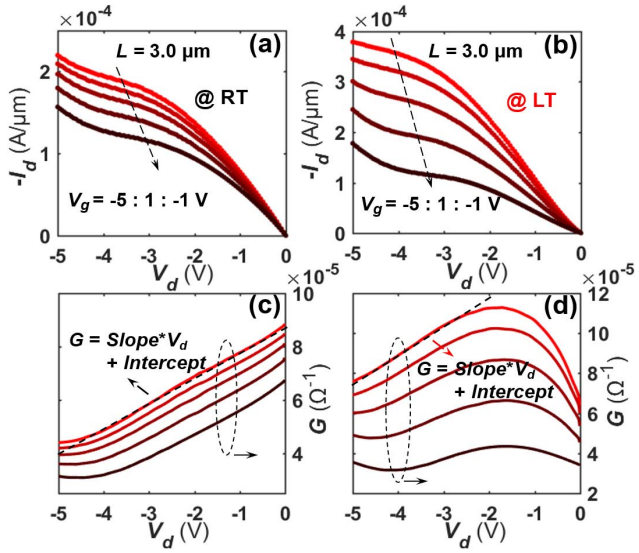

Fig. 1. Output characteristics (a-b) and output conductance G (c-d) of a BP transistor, at RT (298 K) and LT (11 K).

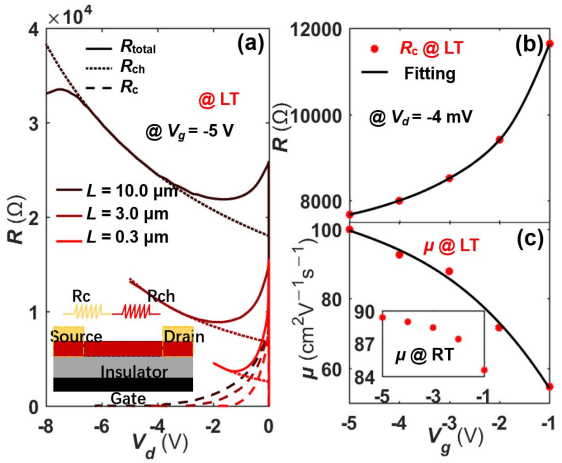

Fig. 2. Contact resistance R_c, channel resistance R_{ch}, mobility μ as a function of drain bias V_d and gate bias V_g, in a BP transistor at LT.

highly demanded for the device modeling and circuit design of 2D transistors [17]–[19].

B. G-Function Model (for Linear and Non-Linear Cases)

In a FET, the total resistance R (*i.e.* $R = 1/G$) is generally regarded as a combination of R_c and R_{ch} (inset to Fig. 2a). R_c is considered as a combination of the interfacial injection resistance $R_{c,int}$ and the bulk injection resistance $R_{c,bulk}$, and mainly modulated by the drain and gate fields, *i.e.* R_c (V_g, V_d) while the source is grounded [11]. R_{ch}, in the above-threshold regime and when $|V_d| < |V_g - V_{th}|$ $|V_{ds}| < |V_g - V_{th}|$, increases with V_d and V_g, *i.e.* R_{ch} (V_g, V_d), as typically expressed by:

$$G_{ch} = \frac{1}{R_{ch}} = C_L \cdot \mu \cdot \left| V_g - V_{th} - \frac{V_d}{2} \right| \tag{1}$$

where $C_L = W{\cdot}C_{OX}/L$, C_{OX} is the gate capacitance per unit area. The channel width W is normalized to be 1 μm in this letter, L is the intrinsic length between source and drain.

In the output characteristics, the dominant effect of R mainly depends on the injection mechanism (Ohmic or Schottky contact) and the external bias V_d. If R_c is negligible or $R_c \ll R_{ch}$ (*i.e.* channel-transport dominant regime), plotting the output conductance G as a function of V_d at a constant V_g, yields $G \cong G_{ch}$ and decreases linearly with V_d [11] (as depicted in Fig. 1c) Therefore, derived from (1), the *Slope*(G, V_d) at a given V_g and *Intercept*(G, V_d) towards $V_d = 0$, are expressed as:

$$|slope\,(G, V_d)| \cong |slope\,(G_{ch}, V_d)| = \frac{C_L \cdot \mu}{2} \tag{2}$$

$$intercept\,(G, V_d) \cong intercept\,(G_{ch}, V_d) = C_L \cdot \mu \cdot (V_g - V_{th}) \tag{3}$$

Practically, large contact resistance can be caused by the Schottky barrier at the metal/semiconductor interface or the interfacial states at the contact interface. This can dominate at a small $|V_d|$ (in Fig. 1d) or in short-channel transistor (*i.e.* contact-injection dominant regime), where R_c becomes non-negligible in comparison with R_{ch}. In such case, direct application of the G-function method without excluding R_c can lead to extraction errors [12], [13]. However, in the linear region of a transistor, by extending the G-function method to higher value range of $|V_d|$, R_{ch} can start to be more dominant than R_c beyond a critical value of V_d (where $R_c = R_{ch}$), so that $R_c \ll R_{ch}$ is valid again (*i.e.* $G \cong G_{ch}$, transition from the injection-dominated to transport-dominated regime) [11], [20]. Therefore, the *Slope* and the *Intercept* equations can still be used, regardless of the contact resistance as well as the injection mechanism.

Both the linear (transport-dominated) and non-linear (injection-dominated) cases of the G-function model, can be fitted by: $G = Slope{*}V_d{+}Intercept$ (Fig. 1c-d). Correspondingly, the $C_L \cdot \mu$ and the V_g-V_{th} parameters are extracted from (2-3); thereafter, the R_{ch} in (1) and R_c can be calculated for both the Ohmic and Schottky contacts in the 2D transistors.

$$R_c = \frac{1}{G} - \frac{1}{|intercept| - |slope| \cdot |V_d|} \tag{4}$$

III. Results Discussion and Model Validation

A. Parameter Extraction and Interpretation

We analyze the output I_d-V_d curves of various BP transistors for different channel length ($L = 0.3, 3.0$ and 10.0 μm) and operation temperatures (RT and LT) by the G-function model, to precisely interpret the device performances and physics. The extracted R_c, R_{ch}, μ versus V_d and V_g at LT are shown in Fig.2, where the large Schottky contact barrier/resistance is presented. R_C at LT is mainly dependent on V_d but relatively weakly dependent on V_g, as follows [11]:

$$R_C\,(V_d) = R_{int,1} \cdot (V_d)^a \cdot \exp(-B_1 \cdot |V_d|^{b1}) \tag{5}$$

where $R_{int,1}$ is the initial R_c, dependent on V_g, the exponential term comes from Schottky barrier injection. The power term $b1$ is related to the local field near the barrier [13], and thereafter extracted to be ~1.26 in this work. B_1 relates to justify the drain field effect to lower the Schottky barrier under the varied L cases, depends on the saturation voltage, *i.e.* $B_1 \propto |V_g - V_{th}|/LB_1 \propto |V_{gs} - V_{th}|/L$. $V_g V_{th} V_{gs} V_{th}$ $V_g - V_{th}$ is respectively extracted to be -2.29, -5.00, -7.54 V at $V_g = -5$ V, for the 3 BP transistors at LT. When V_d is fixed

(*e.g.* $V_d = -4$ mV in Fig. 2b), with the Schottky contact, R_c is derived as follows and independent on L:

$$R_C\left(V_g\right) = R_{int,2}\cdot\exp(-B_2\cdot\left|V_g - V_{th}\right|^{b2}) \quad (6)$$

where $R_{int,2}$ is the initial R_c, dependent on V_d. In this model, $\mathrm{R_{int,1}}\cdot(\mathrm{V_{ds}})^{\mathrm{a}}R_{int,1}\cdot(V_d)^a$ is equal to $R_{int,2}$. At $V_\mathrm{d} = -4$ mV, $R_{int,2}$ is calculated to be $2.83 \times 10^6\Omega$, with the parameter $b2$ fitted to be ~0.8.

In contrast, the Ohmic-like contact is approximately observed at RT, with a total series resistance $R_{c,series}$ which is attributed to the source and drain contacts and decreases with $|\mathrm{V_{ds}}|$ V_d. At $V_d = -4$ mV, $R_{c,series}$ is calculated to be 1049 Ω, whereas the corresponding R_{ch} are respectively 3.37×10^3, 1.12×10^4 and 3.03×10^4 Ω for $L = 0.3$, 3.0 and 10.0 μm. In the long-channel ($L = 3.0$ and 10.0 μm), $R_{c,series}$ can be negligible compared to R_{ch}.

Fig. 2c illustrates the extracted V_g-dependent mobility μ while keeping k constant in (2) for LT and RT and considering the non-zero V_{th}. The μ is fitted with the model: $\mu = \mu_0 \cdot \left|V_g - V_{th}\right|^\beta$ [21], which increases with the carrier density of BP (*e.g.* β in Fig. 2c for BP transistor is extracted to be 1.32) and is inversely proportional to the temperature ($\mu \propto T^{-K}$), and mainly contributed from single-phonon processes [7]. Taking $V_g = -5$ V, the extracted mobility μ at RT is about 85-95 $\mathrm{cm^2V^{-1}s^{-1}}$ for all the L cases, given that the BP transistors were fabricated from the same flake. These values are more reliable than previously discussed in [12], where large variation was observed (*i.e.* the extracted μ at RT varied from 50.7 to 185.0 $\mathrm{cm^2V^{-1}s^{-1}}$, based on the transfer curves and without excluding the effect of contact resistance, *i.e.* using the transconductance method). In overall, the carrier mobility extracted by the G-function model shows good precision and reliability against the effect of contact resistance.

B. Full IV Modeling and Comparison

We model the output characteristics (V_g ranging from −1 to −5 V) of the BP transistors, while implementing the extracted $C_L \cdot \mu$, saturation voltage V_g-V_{th}, channel and contact resistance $R_c(V_g, V_d)$, $R_{ch}(V_g, V_d)$ into the G-function equations. The simulated I_d-V_d curves (colored, bold curves in Figs. 3a-c) fit well with the experimental observations (black, thin curves) at LT (11 K) before the 'up-kink' feature occurred. It validates the good accuracy of the G-function method in the linear regime, with the presence of SBD effect in the BP transistors. Figs. 3d-f illustrate the corresponding G plots and linear fittings, obtained from the experimental characterizations. At RT, the G-function method is also used to interpret and simulate the device output characteristics, showing the good accuracy as well.

To verify the general feasibility of the G-function method, we extend the investigations to other 2D transistors [8], [14], [22], *e.g.* a n-type MoS_2 transistor with $L = 3.0$ μm and 40 nm, at 300 and 4.3 K [8]. The MoS_2 layer was grown by chemical vapor deposition (CVD) on molten glass, then transferred on HfLaO/Si substrate *via* PMMA-assisted transfer strategy [8]. The extraction of R_c, R_{ch} and the I_d-V_d modeling is illustrated in Fig. 4. In the $L = 3.0$ μm, Ohmic contact can be concluded at RT (300 K), from the R_c, R_{ch} plots of Fig. 4a. The SBD effect is observed at LT (4.3 K),

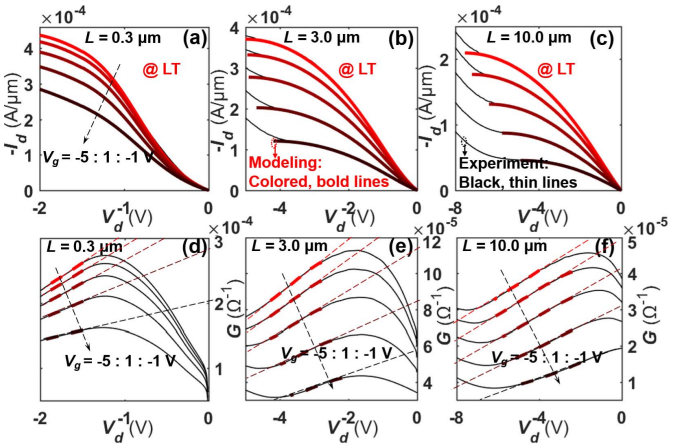

Fig. 3. Output curves modeling (a-c) and conductance interpretation (d-f) *via* G-function in the BP transistors with channel lengths $L = 0.3$, 3.0 and 10.0 μm, at low temperature (LT) of 11 K.

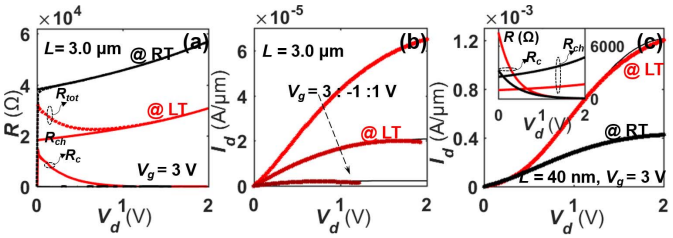

Fig. 4. G-function method in the long- (a-b) and short- (c) channel MoS_2 transistors, with the R_c, R_{ch} extracted from the linear regime and the IV modeling at RT (300 K) and LT (4.3 K).

where the contact-injection dominant regime is presented for $V_d < 0.5$ V. The field-effect mobilities μ extracted at $V_g = 0$ V is consistent with the value of intrinsic mobility in [8], meanwhile the μ at $V_g = 3$ V are obtained to be 77 and 198 $\mathrm{cm^2V^{-1}s^{-1}}$ for the MoS_2 transistor operating at RT and LT, *i.e.* the V_g-dependence [23]. The output curves at LT are simulated and correspondingly fit well with the experiments [8]. In the short-channel ($L = 40$ nm), the R_c can not be ignored for both RT and LT (inset to Fig. 4c), and needs to be taken into account while extracting the device parameters. However, combining with the G-function model, the IV are well reproduced as in Fig. 4c. As well, the G-function method is also demonstrated in other cases, where the SBD effect was resulted from interfacial states and the formation of Schottky contacts, in the n-type MoS2 transistors at RT [14], [22].

IV. Conclusion

In conclusion, based on the output I_d-V_d curves, we extended the G-function method for the 2D transistors (including the n-type and p-type, BP and MoS_2) to correctly interpret the contact R_c and channel resistance R_{ch}, the field-effect mobility μ, the saturation voltage V_g-V_{th} *etc*. The extracted electrical parameters show good accuracy and reliability in understanding the insight physics of the 2D transistor, *e.g.* Schottky-barrier diode effect at 11 K in the BP transistors and in the short-channel MoS_2. Using the numerically modeled μ, V_g-V_{th}, contact and channel resistance $R_c(V_g, V_d)$, $R_{ch}(V_g, V_d)$, the device IV characteristics can be well reproduced, showing its high application potential in future circuit design.

REFERENCES

[1] Y. Liu, J. Guo, E. Zhu, L. Liao, S.-J. Lee, M. Ding, I. Shakir, V. Gambin, Y. Huang, and X. Duan, "Approaching the Schottky–Mott limit in van der Waals metal–semiconductor junctions," *Nature*, vol. 557, no. 7707, pp. 696–700, May 2018, doi: 10.1038/s41586-018-0129-8.

[2] L. Li, Y. Yu, G. J. Ye, Q. Ge, X. Ou, H. Wu, D. Feng, X. H. Chen, and Y. Zhang, "Black phosphorus field-effect transistors," *Nature Nanotechnol.*, vol. 9, no. 5, pp. 372–377, Mar. 2014, doi: 10.1038/NNANO.2014.35.

[3] N. Haratipour, M. C. Robbins, and S. J. Koester, "Black phosphorus p-MOSFETs with 7-nm HfO_2 gate dielectric and low contact resistance," *IEEE Electron Device Lett.*, vol. 36, no. 4, pp. 411–413, Apr. 2015, doi: 10.1109/LED.2015.2407195.

[4] B. Radisavljevic, A. Radenovic, J. Brivio, V. Giacometti, and A. Kis, "Single-layer MoS_2 transistors," *Nature Nanotechnol.*, vol. 6, no. 3, pp. 147–150, Jan. 2011, doi: 10.1038/NNANO.2010.279.

[5] Y. Liu, J. Guo, Q. He, H. Wu, H.-C. Cheng, M. Ding, I. Shakir, V. Gambin, Y. Huang, and X. Duan, "Vertical charge transport and negative transconductance in multilayer molybdenum disulfides," *Nano Lett.*, vol. 17, no. 9, pp. 5495–5501, Aug. 2017, doi: 10.1021/acs.nanolett.7b02161.

[6] Y. Liu, Y. Huang, and X. Duan, "Van der Waals integration before and beyond two-dimensional materials," *Nature*, vol. 567, no. 7748, pp. 323–333, Mar. 2019, doi: 10.1038/s41586-019-1013-x.

[7] A. N. Rudenko, S. Brener, and M. I. Katsnelson, "Intrinsic charge carrier mobility in single-layer black phosphorus," *Phys. Rev. Lett.*, vol. 116, no. 24, pp. 1–6, Jun. 2016, doi: 10.1103/PhysRevLett.116.246401.

[8] Q. Gao, Z. Zhang, X. Xu, J. Song, X. Li, and Y. Wu, "Scalable high performance radio frequency electronics based on large domain bilayer MoS_2," *Nature Commun.*, vol. 9, no. 1, Dec. 2018, Art. no. 4778, doi: 10.1038/s41467-018-07135-8.

[9] M. Estrada, A. Cerdeira, J. Puigdollers, L. Reséndiz, J. Pallares, L. F. Marsal, C. Voz, and B. Iñiguez, "Accurate modeling and parameter extraction method for organic TFTs," *Solid-State Electron.*, vol. 49, no. 6, pp. 1009–1016, Jun. 2005, doi: 10.1016/j.sse.2005.02.004.

[10] Y. Xu, R. Gwoziecki, I. Chartier, R. Coppard, F. Balestra, and G. Ghibaudo, "Modified transmission-line method for contact resistance extraction in organic field-effect transistors," *Appl. Phys. Lett.*, vol. 97, no. 6, Aug. 2010, Art. no. 063302, doi: 10.1063/1.3479476.

[11] C. Liu, T. Minari, Y. Xu, B.-R. Yang, H.-X. Chen, Q. Ke, X. Liu, H. C. Hsiao, C. Y. Lee, and Y.-Y. Noh, "Direct and quantitative understanding of the non-ohmic contact resistance in organic and oxide thin-film transistors," *Organic Electron.*, vol. 27, pp. 253–258, Dec. 2015, doi: 10.1016/j.orgel.2015.09.024.

[12] Y. Xia, G. Li, B. Jiang, Z. Yang, X. Liu, X. Xiao, D. Flandre, C. Wang, Y. Liu, and L. Liao, "Exploring and suppressing the kink effect of black phosphorus field-effect transistors operating in the saturation regime," *Nanoscale*, vol. 11, no. 21, pp. 10420–10428, May 2019, doi: 10.1039/c9nr02907a.

[13] C. Liu, G. Li, R. D. Pietro, J. Huang, Y.-Y. Noh, X. Liu, and T. Minari, "Device physics of contact issues for the overestimation and underestimation of carrier mobility in field-effect transistors," *Phys. Rev. Appl.*, vol. 8, no. 3, Sep. 2017, Art. no. 034020, doi: 10.1103/PhysRevApplied.8.034020.

[14] Y. Sun, D. Xie, X. Zhang, J. Xu, X. Li, X. Li, R. Dai, X. Li, P. Li, X. Gao, and H. Zhu, "Temperature-dependent transport and hysteretic behaviors induced by interfacial states in MoS_2 field-effect transistors with lead-zirconate-titanate ferroelectric gating," *Nanotechnology*, vol. 28, no. 4, Jan. 2017, Art. no. 045204, doi: 10.1088/1361-6528/28/4/045204.

[15] B. Jiang, X. Zou, J. Su, J. Liang, J. Wang, H. Liu, L. Feng, C. Jiang, F. Wang, J. He, and L. Liao, "Impact of thickness on contact issues for pinning effect in black phosphorus field-effect transistors," *Adv. Funct. Mater.*, vol. 28, no. 26, pp. 1–8, 2018, doi: 10.1002/adfm.201801398.

[16] Y. Du, H. Liu, Y. Deng, and P. D. Ye, "Device perspective for black phosphorus field-effect transistors: Contact resistance, ambipolar behavior, and scaling," *ACS Nano*, vol. 8, no. 10, pp. 10035–10042, Oct. 2014, doi: 10.1021/nn502553m.

[17] A. V. Penumatcha, R. B. Salazar, and J. Appenzeller, "Analysing black phosphorus transistors using an analytic Schottky barrier MOSFET model," *Nature Commun.*, vol. 6, no. 1, pp. 1–8, Nov. 2015, doi: 10.1038/ncomms9948.

[18] E. Yarmoghaddam, N. Haratipour, S. J. Koester, and S. Rakheja, "A physics-based compact model for ultrathin black phosphorus FETs—Part I: Effect of contacts, temperature, ambipolarity, and traps," *IEEE Trans. Electron Devices*, vol. 67, no. 1, pp. 389–396, Jan. 2020, doi: 10.1109/TED.2019.2951662.

[19] E. Yarmoghaddam, N. Haratipour, S. J. Koester, and S. Rakheja, "A physics-based compact model for ultrathin black phosphorus FETs—Part II: Model validation against numerical and experimental data," *IEEE Trans. Electron Devices*, vol. 67, no. 1, pp. 397–405, Jan. 2020, doi: 10.1109/TED.2019.2955651.

[20] C. Liu, G. Huseynova, Y. Xu, D. X. Long, W.-T. Park, X. Liu, T. Minari, and Y.-Y. Noh, "Universal diffusion-limited injection and the hook effect in organic thin-film transistors," *Sci. Rep.*, vol. 6, no. 1, pp. 1–14, Jul. 2016, doi: 10.1038/srep29811.

[21] C. H. Kim, A. Castro-Carranza, M. Estrada, A. Cerdeira, Y. Bonnassieux, G. Horowitz, and B. Iniguez, "A compact model for organic field-effect transistors with improved output asymptotic behaviors," *IEEE Trans. Electron Devices*, vol. 60, no. 3, pp. 1136–1141, Mar. 2013, doi: 10.1109/TED.2013.2238676.

[22] X. Xu, Z. Wang, S. Lopatin, M. A. Quevedo-Lopez, and H. N. Alshareef, "Wafer scale quasi single crystalline MoS_2 realized by epitaxial phase conversion," *2D Mater.*, vol. 6, no. 1, Dec. 2018, Art. no. 015030, doi: 10.1088/2053-1583/aaf3e9.

[23] Z. Yu, Z.-Y. Ong, S. Li, J.-B. Xu, G. Zhang, Y.-W. Zhang, Y. Shi, and X. Wang, "Analyzing the carrier mobility in transition-metal dichalcogenide MoS_2 field-effect transistors," *Adv. Funct. Mater.*, vol. 27, no. 19, pp. 1–17, 2017, doi: 10.1002/adfm.201604093.